Phase Behavior of Cholesteryl Ester Dispersions Which Model the Inclusions of Foam Cells†

Julian Snow*
Chemistry Department, Philadelphia College of Pharmacy and Science, Philadelphia, Pennsylvania 19104
Michael C. Phillips
Department of Physiology and Biochemistry, The Medical College of Pennsylvania, Philadelphia, Pennsylvania 19129
Received July 5, 1989; Revised Manuscript Received October 3, 1989

ABSTRACT: In order to understand the phase behavior of the approximately 1-μm-diameter droplets which occur in the cytoplasm of cholesterol-enriched cells, differential scanning calorimetry has been utilized to elucidate the factors controlling the rate of crystallization of cholesteryl esters. The kinetics of the thermotropic transitions between liquid, liquid-crystal, and crystal states which occur in mixtures of cholesteryl oleate and cholesteryl palmitate present in monodisperse, phospholipid-stabilized, emulsion droplets have been determined and are compared to the characteristics of these transitions in bulk mixtures. Cholesteryl palmitate is observed to crystallize in undercooled phospholipid-stabilized dispersions of cholesteryl palmitate/cholesteryl oleate (50/50 w/w) at temperatures up to 50 °C lower than it does in bulk mixtures of the same cholesteryl ester composition. It is postulated that this difference between crystallization temperatures is due primarily to the presence of impurities present in bulk mixtures which act as catalysts that promote crystallization. It is suggested that phospholipid-stabilized dispersions of cholesteryl palmitate/cholesteryl oleate are more appropriate models than bulk mixtures of these cholesteryl esters for studying the kinetic and thermodynamic basis of the phase behavior in cholesteryl ester rich inclusions characteristic of foam cells and atherosclerotic plaque. The thermotropic phase behavior of these dispersions can be satisfactorily analyzed by using the equations of homogeneous nucleation theory. The interfacial tension between the crystal nucleus and the surrounding fluid cholesteryl ester is about 10 erg/cm^2. An equilibrium bulk mixture of 50/50 (w/w) cholesteryl oleate and cholesteryl palmitate at 37 °C contains crystalline cholesteryl palmitate whereas in 1-μm droplets dispersed in an aqueous phase, the cholesteryl palmitate remains in a metastable fluid phase (liquid crystal) for more than 24 h. Consequently, negligible crystallization of saturated cholesteryl palmitate should occur in the inclusions present in the cytoplasm of cells.

Onset of atherosclerosis is characterized by abnormal accumulation of cholesteryl ester (CE)[1] in macrophages and vascular smooth muscle cells of aortic intima. These cells eventually develop into foam cells. Hepatoma cells (Rothblat et al., 1977; Glick et al., 1983; Adelman et al., 1984), smooth muscle cells (Wolfbauer et al., 1986), and macrophages (Brown & Goldstein, 1983) are examples of cultured cell systems which have served as useful models for the study of foam cells. The cellular CE in these systems can be present either in lysosomes or as cytoplasmic inclusions of approximately 1-μm diameter. The cytoplasmic CE is in a dynamic state, continually undergoing a cycle of hydrolysis and reesterification, termed the cholesteryl ester cycle (Brown & Goldstein, 1983). The turnover time of this futile cycle is evidently affected by the physical state of the inclusions. In studies with rat hepatoma cells, hydrolysis of CE in cells with isotropic, liquid inclusions occurred more rapidly than in cells with anisotropic, liquid-crystal inclusions (Glick et al., 1983). The significance of such physical state effects results primarily from its associated effect on the flux of cholesterol between plaque and plasma (Small & Shipley, 1974).

In a previous study, we used DSC to investigate the physical state of CE-rich inclusions isolated from cultured J774 macrophages (Snow et al., 1988). We found that bulk, binary mixtures of CP/CO were useful models for interpreting the equilibrium phase behavior of the isolated inclusions. However, given the turnover dynamics of the CE deposits in cells, it is important to have information about the kinetics of changes in their physical state. In the present study, we have utilized PL-stabilized dispersions of binary CP/CO mixtures in aqueous solution to generate kinetic and thermodynamic data on the phase behavior of these systems. The kinetic analysis, based on classical homogeneous nucleation theory, allows us to predict the time and temperature dependence of the crystallization of CE inclusions of a given size and composition.

Experimental Procedures

Materials. Cholesterol, cholesteryl esters, egg PC, and bovine brain PS were purchased from Sigma Chemical Co. (St. Louis, MO). Cholesteryl oleate and cholesteryl palmitate were recrystallized from 100% ethanol prior to use. HPLC-grade solvents were purchased from Fisher (King of Prussia, PA).

Preparation of CP/CO Dispersions. Stock solutions of CP, CO, PC, and PS were prepared using chloroform [containing 0.75% ethanol]/methanol (2/1 v/v) as solvent. Appropriate amounts of these lipids were added to a 30-mL centrifuge tube, and solvent was evaporated under a stream of nitrogen. Residual solvent was removed under vacuum for at least 2 h. PBS, previously degassed under vacuum for 30 min, was added

† Supported by the National Institutes of Health (Program Project Grant HL 22633).

[1] Abbreviations: CE, cholesteryl ester; CM, cholesteryl myristate; CO, cholesteryl oleate; CP, cholesteryl palmitate; DSC, differential scanning calorimetery; HPLC, high-performance liquid chromatography; PBS, phosphate-buffered saline, pH 7.4; PC, phosphatidylcholine; PL, phospholipid; PS, phosphatidylserine.

0006-2960/90/0429-2464$02.50/0

such that the final mixture contained 20 mL of buffer with a CE content of approximately 0.1% by weight. The PL content was 7% of the total lipid; 80% of the PL was PC and 20% PS. Relatively large amounts of PS were necessary to stabilize the dispersions. The aqueous mixture, subjected to a constant stream of nitrogen, was heated to above the melting temperature of the CE and then sonicated for 30 min. Evaporation of buffer during the sonication was compensated for by adding hot, degassed water to maintain a constant volume. After sonication, glycerol (20% w/v) was added to the hot mixture, which further stabilized the suspension (Mims et al., 1986). Upon cooling, the suspension was filtered through 1–2-μm polycarbonate filters (Nuclepore, Pleasanton, CA).

The CE in the dispersions was analyzed for possible degradation by HPLC (Carroll & Rudel, 1981). A Milton Roy Constametric 3000 HPLC instrument equipped with a Spherisorb ODS2 column, together with a Spectromonitor 3100 and CI 4000 computing integrator, was used for this purpose. Lipid was extracted from the aqueous dispersions with chloroform and the solvent evaporated to dryness under a stream of nitrogen. The lipid was dissolved in tetrahydrofuran/acetonitrile (80:20 v/v) and the column eluted at 1.5 mL/min with acetonitrile/tetrahydrofuran (65:35 v/v). Elution of CE was monitored spectrophotometrically (213 nm).

Differential Scanning Calorimetry. DSC experiments with CP/CO dispersions were conducted with a MicroCal MC-1 or a MicroCal MC-2 scanning microcalorimeter (Northampton, MA) equipped with the downscanning accessory. Data were collected and analyzed with the MC-2 using an IBM PC in conjunction with the MicroCal DA-2 data acquisition and analysis system. Sample concentrations were typically in the range 0.05–0.5% lipid by weight. The samples were scanned against PBS in the reference cells at heating rates of 60 or 90 °C/h and a cooling rate of 25 °C/h. DSC experiments with bulk CE were conducted with a Perkin-Elmer DSC-2 scanning calorimeter (Norwalk, CT). The samples were scanned against empty sample pans; heating rates were typically 5 °C/min, and cooling rates were between 0.62 and 2.5 °C/min. For such experiments, 1–2 mg of lipid was dissolved in approximately 150 μL of chloroform, and the resulting solution was added in small aliquots to 15-μL aluminum sample pans. Solvent was evaporated under a stream of nitrogen. Prior to being sealed, the pans were placed in a vacuum oven at 40 °C for 2 h to remove traces of solvent. Enthalpy calibration was achieved with an indium standard; indium and gallium standards were used for temperature calibration.

The solidification of droplets was analyzed as a first-order process in a manner similar to that of Oliver and Calvert (1975). At a given temperature during a crystallization exotherm, the ratio of the displacement of the curve from the base line to the remaining area under the curve was taken as the first-order rate constant, k, at that temperature. The MC-2 microcalorimeter, which was used for these experiments, measures the rate at which enthalpy is released during the crystallization of the microdroplets. The explicit time dependence of k comes from the numerator of the above ratio, namely, the displacement of the curve from the base line. In this way, the temperature dependence of k was also determined over the temperature range of the exotherm.

Particle Sizing. The size distributions of CE dispersions were determined by photon correlation spectroscopy, using a Coulter N4MD submicron particle analyzer (Hialeah, FL). Fluctuations in scattered light intensity were detected at 90° and analyzed with the on-board Size Distribution Processor

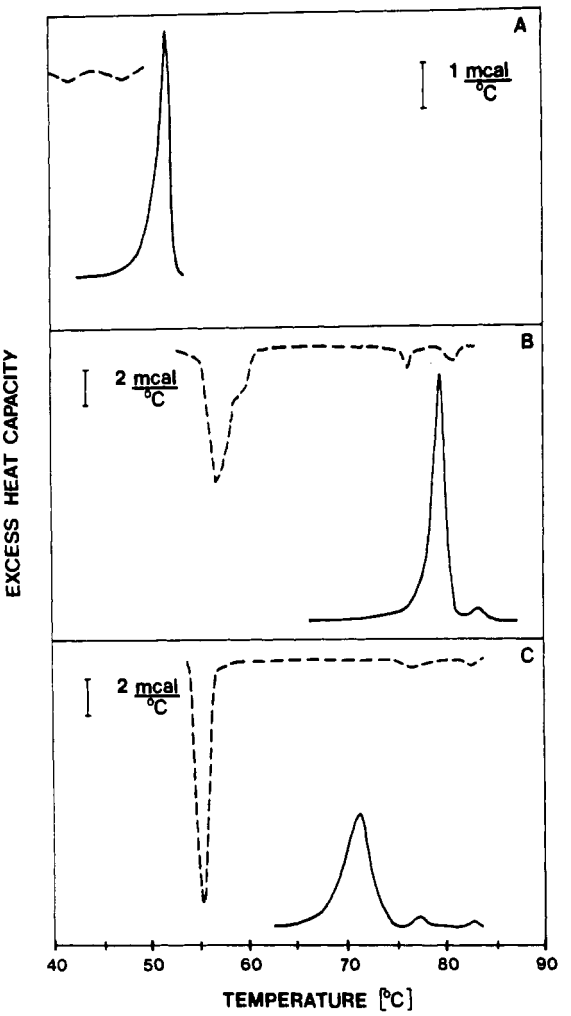

FIGURE 1: Thermotropic behavior of bulk cholesteryl esters. Heat capacity curves are shown for CO (panel A), CP (panel B), and CM (panel C). Heating curves (solid lines) were obtained for samples previously stored at −20 °C overnight. Cooling curves (dashed lines) were obtained after melting the sample and thermostating for 10 min at 5 °C above the melting temperature. The data shown were obtained for a 1-mg sample.

data analysis program. Histograms of the size distributions of the microdroplets were calculated in terms of a weight distribution; 50–100 μL of the suspensions was added to 3–4 mL of PBS, which had been previously filtered through a 0.2-μm filter (Micron Separations, Inc., Westboro, MA). The viscosity and index of refraction of the buffer were taken to be 0.01 P and 1.334, respectively. Data were typically collected for 10 min per run at 25 °C. The computerized analyses of size distributions were not reproducible for samples consisting of more than one population because the peaks were rather broad. These analyses were reproducible, however, for monodisperse samples, so we were careful to develop a methodology which consistently yielded such samples. For different samples in which the PL/CE ratios were equal, the calculated average sizes for monodisperse samples did not differ by more than a few percent from each other.

Results

The phase behavior of several model CE systems was studied using DSC. These model systems consisted of either a single CE component or binary CE mixtures. The systems were examined in bulk form and as microdroplets dispersed in phosphate-buffered saline (PBS), pH 7.4.

Figure 1A shows heat capacity curves for bulk CO obtained upon heating (solid line) and cooling (dashed line). The single

endotherm in the heating curve indicates that crystalline CO melts to form an isotropic liquid at about 51 °C. Both the experimental melting point and heat of fusion, obtained by integrating the area underneath this peak, agree closely with literature values (T_m = 51 °C, ΔH_{fus} = 5.60 kcal/mol). The values for T_m and ΔH_{fus} quoted here and subsequently for other CE are the literature values of Ginsburg et al. (1984). In all cases, our experimental values for T_m and ΔH_{fus} were within 1 °C and 5%, respectively, of the literature values. The dashed line in Figure 1 indicates that the CO solid–isotropic liquid phase transition is not reversible; cooling the melted sample results in formation of two liquid-crystalline phases (mesophases) at somewhat lower temperatures than the crystalline–isotropic liquid phase transition obtained upon heating, and each is associated with considerably less enthalpy (about 1 cal/g). An exothermic, isotropic liquid–cholesteric liquid-crystalline exothermic transition occurs at about 47 °C, and a cholesteric–smectic liquid-crystalline transition occurs at about 43 °C (Ginsburg et al., 1984). Since the liquid-crystalline phases observed upon cooling form at temperatures lower than the normal melting temperature, T_m, and since they are thermodynamically less than the crystalline phases at these temperatures, they are metastable (Ginsburg et al., 1984). Further cooling of the sample induces no observable crystallization, even down to temperatures close to 0 °C (data not shown). That no observable crystallization occurred upon supercooling this sample to such a low temperature suggests that a sizable activation energy barrier between the liquid-crystalline and crystalline phases exists (see Discussion). The apparent lack of crystallization at low temperatures may also be due to the removal of impurities by careful crystallization from ethanol (see Experimental Procedures). However, it should be noted that a crystal–isotropic liquid melting endotherm is typically observed upon reheating such supercooled samples, which indicates that some recrystallization had occurred during the cooling scan and/or immediately prior to reheating.

Heat capacity curves for melting and cooling bulk CP are shown in Figure 1B. Crystalline CP melts (solid line) to form a stable cholesteric liquid-crystalline phase at about 80 °C (ΔH_{fus} = 14.6 kcal/mol; Ginsburg et al., 1984), and a cholesteric–isotropic liquid transition occurs at about 83 °C. Upon cooling (dashed line), the isotropic liquid–cholesteric liquid-crystalline transition occurs at about 82 °C, and the cholesteric–smectic liquid-crystalline transition occurs near 77 °C. The smectic phase is metastable. The large exotherm centered near 57 °C indicates that crystallization of bulk CP occurs in this temperature range. The existence of a shoulder on the high-temperature side of this exotherm provides evidence for the occurrence of a polymorphic transformation (Ginsburg et al., 1984). For cooling rates between 2.5 and 10 °C/min, corrections must be made for thermal lag. Ideally, lower cooling rates should be used; however, it was not possible to use the lower scan rates for all samples because the instrument lacks the necessary sensitivity. Although we used the lowest cooling rates possible (as low as 0.62 °C/min), we did not attempt to correct for thermal lag for two reasons: for bulk samples, we were only qualitatively interested in crystallization temperatures; also, for bulk samples, crystallization temperatures are not reproducible to more than a few degrees centrigrade, probably because crystallization is due to heterogeneous nucleation (see Discussion). Undercooling can be expressed by defining a dimensionless parameter, the reduced critical undercooling parameter, $\Delta T_c/T_m = (T_m - T_c)/T_m$, where T_m is the melting point (degrees kelvin) and T_c is the temperature (degrees kelvin) below which the sample cannot be cooled without rapid crystallization occurring. For bulk CP, this parameter is 0.065 (Figure 1B).

Figure 1C shows the heating and cooling curves for bulk CM. The phase behavior of this CE was studied because, like CP, it has a fully saturated fatty acyl chain (14:0) and relatively high T_m and ΔH_{fus} (11.4 kcal/mol; Ginsburg et al., 1984). However, unlike CP, there are no known polymorphic crystalline forms for CM. Crystalline CM (solid line) melts near 72 °C to form a smectic liquid-crystalline phase. The smectic–cholesteric liquid-crystalline and cholesteric liquid-crystal–isotropic liquid transitions occur near 77 and 83 °C, respectively. The cooling curve (dashed line) indicates that undercooling by approximately 17 °C is necessary for crystallization to occur and that crystallization is preceded by formation of cholesteric and smectic liquid-crystalline phases ($\Delta T_c/T_m$ = 0.049).

A comparison of the cooling curves obtained for bulk CO and CP is of interest. Pure, melted CO can be undercooled up to 50 °C with no appreciable crystallization occurring, whereas bulk CP begins to crystallize after being undercooled less than 25 °C. Consequently, it is reasonable to expect that CO could exist for prolonged periods of time in a metastable, liquid-crystalline state at physiological temperatures, whereas CP should crystallize readily. Given these differences, we determined the effects of undercooling bulk, binary mixtures of CP/CO. Such mixtures are of particular interest, since CP and CO are major components of the CE deposited in foam cells and atherosclerotic plaque (Katz & Small, 1980; Lundberg, 1985).

CP/CO forms a simple eutectic system whose phase diagram has been published elsewhere (Small, 1986; Snow et al., 1988) and is reproduced in Figure 2A. This figure is actually composed of two phase diagrams superimposed on one another. The diagram represented by filled circles, squares, and triangles and by solid lines depicts crystalline transitions. The eutectic point (E, 49–50 °C, 83–84% CO by weight) corresponds to the minimum melting point of any CP/CO mixture and is invariant (three phases coexist at this point). Crystalline samples of any other composition will partially melt to form a liquid with the eutectic composition (●). The remaining solid, either CP or CO, melts at higher temperatures (■); for mixtures containing less than 83–84 % CO, the remaining solid will be pure CP. The points (▲) correspond to solid–solid transitions which occur only for samples whose composition is close to the eutectic composition. The dashed lines and open circles and squares represent liquid-crystalline transitions and were obtained by cooling melted samples several degrees below the lowest liquid-crystalline transition and then reheating them before crystallization occurred. The points (□) represent cholesteric liquid-crystalline–isotropic liquid transitions and the points (○) smectic–cholesteric liquid-crystalline transitions. The smectic phase is seen to be metastable for all compositions, whereas the cholesteric phase is metastable only for CO compositions between approximately 15–70% and greater than 90%. During the initial melt, for samples with CO compositions between approximately 0–15% and 70–90%, the sample melts to form a stable cholesteric liquid crystal, which then melts to form an isotropic liquid.

Figure 3A shows heating and cooling curves for a bulk, binary mixture of CP/CO (50/50 w/w = 50/48 mol/mol). According to the interpretation of the phase diagram given above, the peak (solid line) centered near 47 °C is due to melting of part of the crystalline CP and all of the crystalline CO present to form a CO-rich liquid with the eutectic com-

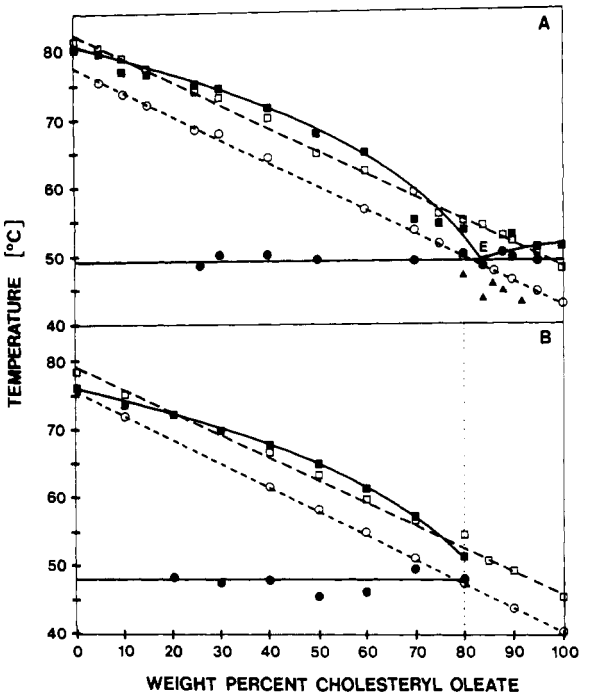

FIGURE 2: Condensed binary phase diagrams for CP/CO. (Panel A) Phase diagram for bulk mixtures; (panel B) phase diagram for PL-stabilized dispersions of CP/CO mixtures in PBS with 20% (w/v) glycerol. The continuous curves representing fits through (●) and (■) were obtained during initial heating scans and represent melting of solid phases of CP/CO to either an isotropic liquid (■) or a liquid of eutectic (E) composition (83–84% CO) (●). The liquid of eutectic composition coexists with either solid CP (CO <83–84%) or solid CO (CO >83–84%). The dashed lines representing fits through (○) and (□) were obtained by cooling the samples and reheating before crystallization occurred. (○) Temperatures of transitions from the smectic liquid-crystalline phase to the cholesteric liquid-crystal; (□) temperatures of transitions from the cholesteric liquid-crystalline phase to the isotropic liquid. The points designated (▲) represent solid–solid transitions. No crystalline transitions were observed for PL-stabilized dispersions with compositions represented by values on the abscissa to the right of the vertical dashed line (panel B). The temperatures are peak temperature of transitions observed calorimetrically: (panel A) 5 °C/min (Perkin-Elmer DSC-2); (panel B) 1 °C/min (MicroCal MC-1).

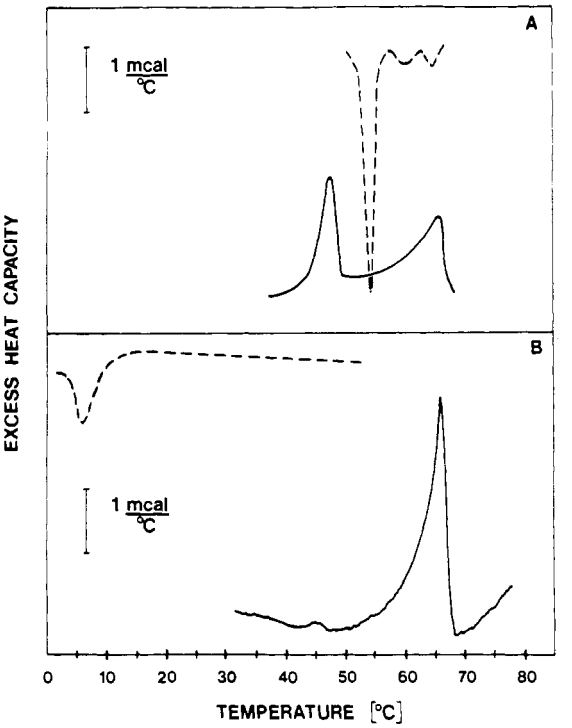

FIGURE 3: Thermotropic behavior of CP/CO (50/50) mixtures. (Panel A) Heat capacity curves for bulk CP/CO and (panel B) PL-stabilized dispersions of CP/CO in PBS with 20% (w/v) glycerol. The data shown in panel A were obtained for a 1-mg sample. Heating curves (solid lines) for bulk mixtures were obtained for samples previously cooled to −20 °C overnight. Dispersions were refrigerated at 4 °C overnight prior to heating. All samples were maintained at 75 °C for 10 min prior to obtaining cooling curves.

position. The peak centered near 65 °C is due to melting of excess CP. Cooling the melted mixture (dashed line) results in the initial formation of two metastable liquid-crystalline phases, followed by crystallization of pure CP near 55 °C. It is interesting to note that crystallization of pure CP occurs in the CP/CO mixture within a few degrees of crystallization of CP in pure CP samples and that the polymorphism observed in Figure 1B for undercooling pure CP is not observed for the mixture.

Bulk samples are convenient to work with and were useful models for interpreting the equilibrium thermodynamic properties of CE-rich inclusions isolated from cultured J774 macrophages (Snow et al., 1988). These inclusions are actually microdroplets of lipid surrounded by a phospholipid monolayer, which effectively disperses the CE in an aqueous environment. For this reason, CP/CO mixtures dispersed with phospholipid in PBS were prepared, as they were expected to be more realistic models than bulk mixtures. Care was taken to develop a methodology that resulted in the preparation of droplets of a uniform size since this greatly facilitated the kinetic analysis of the cooling curves (see Discussion). The size distributions of the samples were analyzed by photon correlation spectroscopy (see Experimental Procedures), and these were typically found to be unimodal (Figure 4), with an average diameter of slightly less than 1 μm. Since the preparation of these dispersions involved extensive sonication at elevated temperatures, lipids were extracted from representative samples and analyzed for possible degradation by HPLC (see Experimental Procedures). No degradation was observed to occur relative to control samples, which were prepared from the stock CE solutions with no sonication.

Figure 3B shows heating and cooling curves, respectively, for PL-stabilized dispersions of CP/CO (50/50 w/w). The average diameter of droplets in this sample was 0.7 ± 0.4 (SD) μm. The heating curve for a dilute suspension of these droplets (solid line, Figure 3B) shows a single large endotherm centered near 65 °C, corresponding to melting pure CP. A small peak near 46 °C, corresponding to the initial, partial melt to form isotropic liquid of the eutectic composition, is smaller than would be expected for a bulk sample (Figure 3A). However, the base behavior of CP/CO mixtures depends on the thermal history of the sample, and evidently the CO in this sample was initially present in a long-lived, fluid (liquid-crystalline) state.

The cooling curve for the CP/CO dispersions (dashed line, Figure 3B) shows an exotherm centered near 6 °C, corresponding to crystallization of CP. This result is strikingly different from that obtained for bulk CP/CO of the same CE composition (Figure 3A, dashed line), in which CP was observed to crystallize near 55 °C ($\Delta T_c/T_m = 0.03$). Dispersing the CP/CO mixture clearly enhanced the metastability of the liquid-crystalline CP relative to bulk behavior ($\Delta T_c/T_m = 0.17$). It is also clear from this cooling curve that the enthalpy released during crystallization of CP from the CP/CO (50/50) mixture is somewhat less than the enthalpy absorbed during melting of the CP (solid line, Figure 3B). Although it is not apparent why these values are unequal, it is important to note that there is very little crystallization at higher temperatures, as is shown by the flat high-temperature base line. The dif-

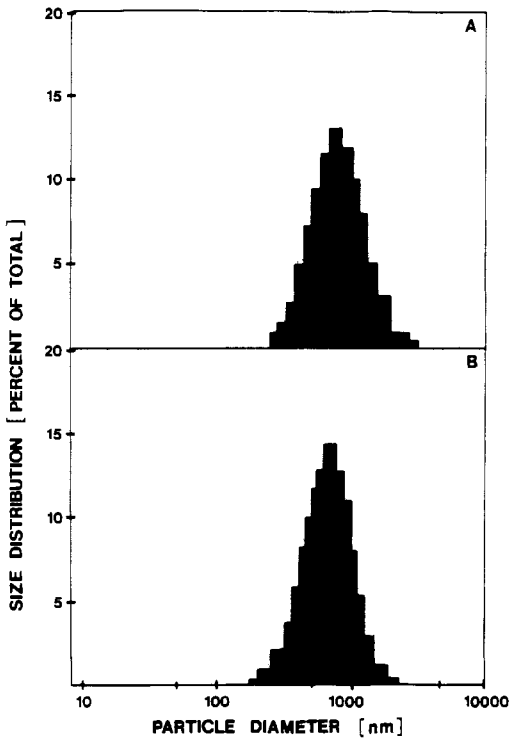

FIGURE 4: Histogram depicting size distributions for PL-stabilized dispersions of CP/CO (50/50) (panel A) and CM (panel B). The abscissa shows the log scale range of sizes in nanometers. Scattered light intensity was related to size on a weight percent basis according to the Size Distribution Processor data analysis program of the Coulter N4MD submicron particle analyzer. The results were divided into log scale subranges, and the size within each subrange was presented as a percent of the total on the ordinate.

ference in enthalpy may be a function of the cooling rate, and we are investigating this, although it is difficult to obtain data at slower cooling rates than used in this study because of limitations in instrument sensitivity. We were able to show that varying the amount of glycerol, which was added to stabilize the dispersions (see Experimental Procedures), from 5 to 20% (w/v) resulted in no detectable change in the melting behavior of the lipid. The exotherms observed during cooling were shifted by no more than 1 °C over this range of added glycerol (data not shown). That glycerol has a negligible effect on the thermal properties of the CE is expected on the basis of the hydrophilic nature of glycerol.

The enhanced metastability of liquid-crystalline CP noted in Figure 3B is further illustrated in Figure 2B, which shows a binary phase diagram for dispersed CP/CO. This phase diagram is very similar to that obtained for bulk CP/CO (Figure 2A), although there are some interesting differences. Samples containing less than 80% CO typically exhibited two crystalline transitions during the initial heating scan. A partial melt occurred near 48 °C in these samples to form a CO-rich liquid of the eutectic composition. Excess CP melted subsequently at temperatures dependent on the varying amount of CO present in the liquid phase. The liquid-crystalline transitions, obtained during the second heating scan, were similar to those observed for bulk CP/CO mixtures. The phase diagram for CP/CO dispersions appears to be shifted to slightly lower temperatures by about 1 °C relative to the bulk CP/CO phase diagram. Furthermore, notice that in the phase diagram for bulk CP/CO (Figure 2A) the solidus line representing melting of CP (■) intersects the left-hand ordinate (100% CP) near 80 °C, the T_m of the higher melting polymorph of CP. For PL-stabilized dispersions, the analogous intersection on the phase diagram occurs near 76 °C, which is close to the T_m value for the lower melting polymorph for CP (Ginsburg et al., 1984). The data suggest that the lower melting polymorph for CP is relatively more stable for dispersed CP/CO than it is for bulk CP/CO. The major differences between these phase diagrams are observed for mixtures whose CO composition exceeds 80%. For CP/CO dispersions with such compositions, only liquid-crystalline transitions were observed, even after refrigerating the samples for up to 1 week at 4 °C. Evidently, the metastability of these CO-rich dispersions was enhanced considerably relative to bulk mixtures with the same composition. These results are consistent with two interesting observations noted previously: bulk, fluid CO, with a relatively low heat of fusion and T_m, can be undercooled to a much greater extent without inducing crystallization than can bulk CP, with a relatively large heat of fusion and high T_m (cf. Figure 1A,B). Furthermore, dispersed mixtures of fluid CP/CO can be undercooled to a much greater extent than bulk CP/CO mixtures of the same CE composition without inducing crystallization (cf. Figure 3A,B, dashed lines). It is not surprising, then, that dispersed CP/CO mixtures rich in CO should exhibit enhanced fluidity relative to bulk CP/CO mixtures of the same CE composition. Interestingly, liquid-crystalline mixtures (bulk) with the eutectic composition are even less likely to crystallize at low temperatures than pure CO dispersions.

Since our objective is to understand the thermodynamics and kinetics of the phase behavior of CE-rich inclusions found in atherosclerotic foam cells, it is important to determine the fraction of CE in a microdroplet that remains uncrystallized as a function of time at physiological temperature (37 °C). To this end, dispersions of CP/CO (50/50 w/w) were heated to 70 °C to melt the microdroplets and remove crystalline material, then cooled and held at 37 °C in the calorimeter for 24 h, and then reheated. The resulting heat capacity curve showed no cooperative transition up to 75 °C (data not shown), indicating that crystallization had not occurred during the 24 h at 37 °C.

Cooling curves for dispersed CO exhibited no exotherms at temperatures approaching 0 °C, which is consistent with results observed for bulk CO (Figure 1A). In contrast, saturated CE in dispersion might be expected to crystallize above 0 °C (cf. Figure 1B for CP). Dispersed samples of CM were chosen for such studies because, unlike CP, this CE exhibits no polymorphic behavior upon cooling. The heating and cooling curves for a monodisperse suspension of CM (average diameter = 0.7 ± 0.4 μm) are shown in Figure 5. The heating curve (solid line) is very similar to that obtained for bulk CM (Figure 1C, solid line), as expected. The cooling curve, with an exotherm centered near 11 °C, shows that dispersed CM can be undercooled nearly 45 °C more than bulk CM (Figure 1C, dashed line) before crystallization occurs ($\Delta T_c/T_m = 0.17$). The enthalpy released upon crystallization of dispersed CM is less than the enthalpy absorbed during melting, behavior similar to that of CP in CP/CO mixtures discussed above (Figure 3B).

Discussion

The phenomenon of undercooling is typically minimized in bulk samples because impurities are presumably present which serve as accidental catalytic centers that lead to heterogeneous nucleation (Turnbull, 1952). This explains why CP crystallizes at 55 °C in bulk mixtures of CP/CO (50/50 w/w) but must be cooled to 6 °C before crystallization occurs in dispersed mixtures (Figure 3A,B). The results shown in Figure 1A for bulk CO, however, indicate that heterogeneous nucleation apparently does not have a dominant effect on the crystalli-

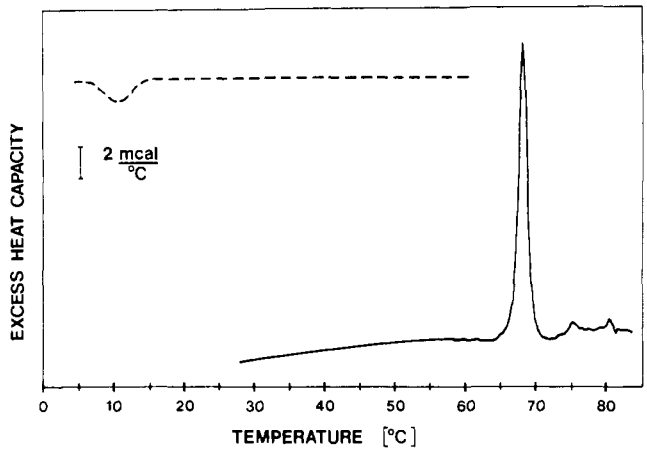

FIGURE 5: Thermotropic behavior for PL-stabilized dispersions of CM in PBS with 20% (w/v) glycerol. See legend of Figure 3 for details.

zation of CO since a significant amount of undercooling was observed with this sample.

Useful information has been obtained by applying the equations of nucleation theory to the analysis of such undercooling phenomena. However, with the exception of bulk CO, crystallization of all other bulk samples studied was due to heterogeneous nucleation. The ratios $\Delta T_c/T_m$ for these samples were considerably lower (0.03–0.065) than those typically observed for homogeneous nucleation (0.13–0.37; Oliver & Calvert, 1975). In early work in this field, the sample mass was typically broken into a number of isolated droplets with an emulsifying agent to minimize the possibility of heterogeneous nucleation. Several systems have been studied successfully using this approach, including triglycerides (Skoda & Van den Tempel, 1963; Phipps, 1964).

Intuitively, one would expect the increased metastability of CO relative to both CP and CM to be due to the low T_m and heat of fusion values for CO relative to those values for CP and CM. This observation is correct and is given quantitative expression by homogeneous nucleation theory (Volmer & Weber, 1925; Becker & Doring, 1935; Turnbull & Fisher, 1949). The theory also explains the observed effects of dispersing the lipid. Briefly, in the absence of impurities, formation of a new phase upon cooling is preceded by formation of small molecular clusters of the new phase, or nuclei. Growth of these clusters occurs slowly until nuclei of a critical size are reached; subsequent growth of nuclei, followed by crystallization, occurs rapidly. Nucleation is assumed to proceed according to absolute rate theory (Eyring & Eyring, 1963); accordingly, the rate constant, I, for nucleus growth is

$$I = (\text{constant})\frac{kT}{h}\exp\left(-\frac{\Delta G^*}{kT}\right) \quad (1)$$

where ΔG^* is an activation free energy change required to form a nucleus of critical size (erg) and k and h are Boltzmann's and Planck's constants, respectively. ΔG^* consists of a surface free energy term associated with forming the interface between the nucleus and the surrounding fluid, and a bulk free energy of fusion associated with forming the interior of the nucleus. The former contribution is positive in sign and impedes growth. The latter contribution, ΔG_v (ergs per cubic centimeter), is

$$\Delta G_v = \Delta H_v - T\Delta S_v$$

where ΔH_v (ergs per cubic centimeter) and ΔS_v (ergs per cubic centimeter per degrees kelvin) are the enthalpy and entropy of fusion, respectively, per unit volume. Assuming ΔS_v is approximately equal to $\Delta H_v/T_m$, then

$$\Delta G_v = \Delta H_v(\Delta T/T_m) \quad (2)$$

and ΔG_v only becomes negative when ΔT is positive (i.e., T is less than T_m) because ΔH_v is always negative. This explains, in general, why undercooling is necessary for crystallization to occur (in the absence of impurities). It is interesting to note that liquid-crystalline transitions typically occur near the same temperature both on heating and on cooling (i.e., ΔT is small). This must mean that the activation energies for formation of these mesophases is considerably less than the activation energy for crystallization. The final expression for ΔG^* is (Fisher et al., 1949)

$$\Delta G^* = a\sigma^3/\Delta G_v^3 \quad (3)$$

where a is a form factor depending on the shape of the nucleus ($16\pi/3$ for a sperical nucleus) and σ is the interfacial tension between the crystal nucleus and surrounding fluid (ergs per square centimeter). The result of the Turnbull–Fisher analysis may be written as

$$I = A\exp\left(-\frac{a\sigma^3 T_m^2}{\Delta H_v \Delta T^2 kT}\right) \quad (4)$$

where I is the frequency of formation of crystal nuclei/volume of undercooled fluid. A, the preexponential factor, has a temperature dependence which others have demonstrated to be negligible (Turnbull, 1952; Skoda & Van den Tempel, 1963).

It was mentioned previously that PL-stabilized dispersions of CE mixtures were expected to constitute a physiologically more relevant model than bulk mixtures for the CE-rich inclusions that characterize foam cells and atherosclerotic plaque. Accordingly, kinetic analyses of the crystallization behavior for dispersed mixtures of CP/CO (50/50 w/w) (Figure 3A, dashed line), and also for CM (Figure 5, dashed line), were performed using the equations of nucleation theory (Turnbull, 1952). According to the theory, it is assumed that the rate of solidification of droplets of diameter D is first order with respect to the total volume, V_D, of fluid remaining in all such droplets at time t, so

$$-\frac{dV_D}{dt} = k_D V_D \quad (5)$$

where k_D is the first-order rate constant (min^{-1}). The total volume rate of solidification would then be

$$-\frac{dV}{dt} = \sum_{D=0}^{\infty} k_D V_D = \int_0^{\infty} k_D V_D \, dD \quad (6)$$

The use of monodisperse samples of CE-containing microdroplets whose diameter varied symmetrically about an average value D simplified the calculations considerably because it avoided the need to perform the summation indicated in eq 6; instead, we were able to use eq 5 with k_D and V_D corresponding to all droplets of average diameter D. The time dependence of k_D can be obtained from the cooling curves as described under Experimental Procedures. k_D is related to I (eq 4) by the equation $k_D = Iv_D$, assuming homogeneous nucleation occurs, where v_D is the volume of a droplet of average diameter D (Turnbull, 1952; Skoda & Van den Tempel, 1963).

Since all the dispersions used in the kinetic analyses consisted of a homogeneous size population, it follows that crystallization of each sample could be characterized by a single first-order rate constant, k_D. Also, since I is calculated by using the equation $k_D = Iv_D$, ln I should be linearly related to $1/\Delta T^2 T$ (eq 4). Figure 6 shows such a linear relationship

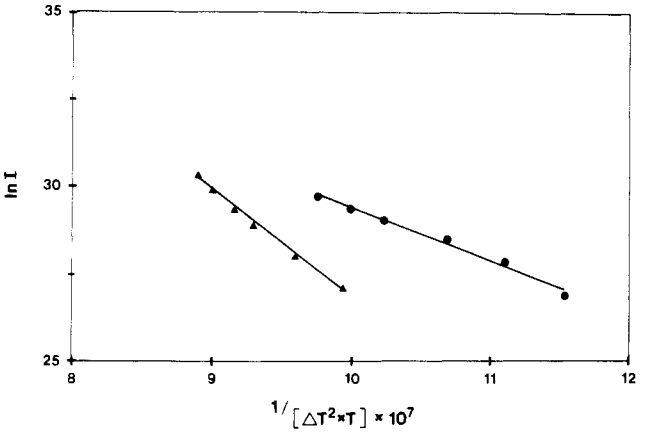

FIGURE 6: Crystallization kinetics for PL-stabilized dispersions of CP/CO [50/50 (▲)] and CM (●) in PBS with 20% glycerol (w/v). Data are presented as ln I vs $1/\Delta T^2T$ according to eq 4. I, the rate of nucleation per cm^3 of supercooled CE, was evaluated from the crystallization exotherms observed calorimetrically. $\Delta T = T_m - T$.

for dispersions of CP/CO (50/50 w/w) and for dispersions of CM. Values for σ, calculated from the slopes of these lines, were 13.1 and 8.6 erg/cm^2 for CP/CO and CM dispersions, respectively. These parameters were calculated by using estimated densities of 1.02 and 0.97 g/cm^3 for smectic liquid-crystalline CP and CM, respectively (Small, 1986). The values for σ obtained in this study are similar to values of this parameter obtained by others for emulsified triglycerides (Skoda & Van den Tempel, 1963) and for several normal alkanes (Oliver & Calvert, 1975).

The foregoing analysis shows that the metastability of undercooled dispersions of both CP/CO (50/50 w/w) and of CM can be explained satisfactorily by using the equations of classical nucleation theory. It should be pointed out, however, that the linear relationship between ln I and $1/\Delta T^2T$ does not preclude the possibility that heterogeneous nucleation has occurred, even though the observed values for $\Delta T_c/T_m$ are large enough to indicate that homogeneous nucleation was likely. For example, even in the absence of catalytic impurities in the CE core of a microdroplet, the fatty acyl chains of the PL monolayer surrounding the microdroplet could act as a (heterogeneous) catalyst. Experiments designed to elucidate the influence of PL on the crystallization behavior of CE microdroplets will be included in future studies. The fact that we have not ruled out the possibility of heterogeneous nucleation does not detract significantly from the above conclusions; as long as the microdroplets in question are of similar size, only minor corrections are necessary, since the temperature dependencies predicted for both homogeneous and such heterogeneous nucleation are identical (Turnbull, 1952).

It is of interest to note that the degrees of undercooling observed for dispersions of both CP/CO (50/50 w/w) and CM were similar ($\Delta T_c/T_m = 0.17$ for both). Assuming that the phase behavior of CM approximates that of CP, the most important influence of the CO in promoting fluidity in binary mixtures of CP/CO would seem to be a colligative effect, namely, to lower the melting temperature of the CP. Since $\Delta T_c/T_m$ is approximately constant, the onset of crystallization both of CM in CM dispersions and of CP in CP/CO dispersions is determined by the melting temperature of CM and CP, respectively ($T_c = 0.83T_m$ in both cases). In the latter case, T_m for CP is lowered by approximately 15 °C (cf. Figures 2B and 3B) due to the presence of the impurity, CO.

A distinct advantage of having an appropriate theoretical model to explain the observed undercooling phenomena is that it allows us to predict the time and temperature dependence of the metastability of liquid-crystalline microdroplets of similar composition. It is of interest to predict the fraction of CP that remains uncrystallized after 24 h at 37 °C. Brown et al. have shown that this is the half-time for hydrolysis and reesterification of CO in mouse peritoneal macrophages (1980). It has also been demonstrated that cellular CE clearance depends on the physical state of the stored CE. Studies using Fu5AH rat hepatoma cells showed that CE clearance from cells containing liquid, isotropic CE-rich inclusions occurred almost twice as rapidly as CE clearance from cells with anisotropic inclusions (Glick et al., 1983). These studies indicate the importance of the metastability of liquid-crystalline states in maintaining fluidity in systems for which the crystalline state is thermodynamically more stable. Since the cellular CE is in a dynamic state due to the cholesteryl ester cycle, 24 h would appear to be a minimal time period required to maintain a fluid, metastable state, since 50% of the CE undergoes a cycle of hydrolysis and reesterification in that time period under steady-state conditions. Presumably, freshly esterified CE is deposited in a fluid state since the long-range structure which characterizes the crystalline state would initially be absent. The time and temperature dependence for crystallization of CP in CP/CO mixtures can be obtained by integrating eq 5, using the relationship $k_D = Iv_D$, and then substituting the expression in eq 4 for I. A value for σ is taken from the slope of the straight line in Figure 6 (▲). The results of performing such calculations indicate that nearly 100% of the CP in approximately 1-μm droplets of CP/CO (50/50 w/w) should remain in a relatively fluid liquid-crystalline state after 24 h at 37 °C. The calorimetric experiments in which dispersions of fluid CP/CO (50/50 w/w) were held at 37 °C for 1 day prior to reheating confirm this theoretical prediction. Furthermore, it is easy to demonstrate that at 37 °C negligible crystallization of this mixture will occur in any biologically significant time period.

Temperature has a dramatic effect on the rate of solidification. Thus, the exotherm corresponding to crystallization of CP/CO (50/50 w/w) dispersions (Figure 3) is centered near 6 °C, and 50% of the CE crystallizes within minutes at this temperature. However, the theoretical analysis predicts that at 11 °C it would take about 21 h for 50% of the CE to crystallize, while at 16 °C it would take almost 2 years. These temperature effects are largely due to the exponential dependence of I on the inverse square of ΔT (eq 4). A relatively small increase in T decreases ΔT, resulting in a very large decrease in the nucleation rate. It is interesting to notice that in PL-stabilized dispersions, CP apparently crystallizes to its lower melting polymorph (cf. Figure 2A,B). This means that ΔT will be about 4–5 °C lower at any given temperature less than T_m than it would be if CP were to crystallize to its higher melting polymorph. This results in a very large decrease in the nucleation rate as can be seen from the examples given above.

In an earlier study, we examined the phase behavior of CE-rich inclusions isolated from cultured J774 macrophages (Snow et al., 1988). These inclusions contained CP and CO as the predominant CE, in approximately a 50/50 (w/w) ratio. It was found that bulk, binary mixtures of CP/CO were useful models for understanding the thermodynamic basis of the phase behavior of the cellular inclusions. The results of this work suggested that microcrystals of CP existed within these inclusions. However, it was pointed out that the thermal history of the inclusions was important with regard to this phase behavior and that this parameter could not be controlled with absolute certainty.

Although bulk CE mixtures are good models for interpreting the equilibrium thermodynamic properties of cellular CE-rich inclusions, the present study has shown that heterogeneous nucleation of undercooled, fluid lipid occurs with bulk mixtures; hence, these mixtures are poor models for studying the kinetic properties of the phase behavior of cellular inclusions. CE dispersions consisting of microdroplets with approximately the same average diameter as that of the cellular inclusions constitute a more appropriate model for predicting the time dependence of the cellular lipid phase changes because homogeneous nucleation occurs. The present study suggests that in cells at 37 °C CP within inclusions containing up to 50% CP should be liquid crystalline (or liquid) under steady-state conditions.

ACKNOWLEDGMENTS

We express our gratitude to Dr. John F. Brandts (University of Massachusetts, Amherst) for his generous offer to use the facilities at MicroCal, Inc. (Northampton, MA), for several of our experiments. We also thank his engineer, Sam Williston, for his assistance.

Registry No. Cholesteryl oleate, 303-43-5; cholesteryl palmitate, 601-34-3.

REFERENCES

Adelman, S. J., Glick, J. M., Phillips, M. C., & Rothblat, G. H. (1984) *J. Biol. Chem. 259*, 13844–13850.
Becker, R., & Doring, W. (1935) *Ann. Phys. 24*, 719–731.
Brown, M. S., & Goldstein, J. L. (1983) *Annu. Rev. Biochem. 52*, 223–261.
Brown, M. S., Ho, Y. K., & Goldstein, J. L. (1980) *J. Biol. Chem. 255*, 9344–9352.
Carroll, R. M., & Rudel, L. L. (1981) *J. Lipid Res. 22*, 359–363.
Eyring, H., & Eyring, E. M. (1963) *Modern Chemical Kinetics*, Reinhold Publishing Co., New York.
Ginsburg, G. S., Atkinson, D., & Small, D. M. (1984) *Prog. Lipid Res. 23*, 135–167.
Glick, J. M., Adelman, S. J., Phillips, M. C., & Rothblat, G. H. (1983) *J. Biol. Chem. 258*, 13425–13430.
Katz, S. S., & Small, D. M. (1980) *J. Biol. Chem. 255*, 9753–9759.
Lundberg, B. (1985) *Atherosclerosis (Shannon, Irel.) 56*, 93–110.
Mims, M. P., Guyton, J. R., & Morrisett, J. P. (1986) *Biochemistry 25*, 474–483.
Oliver, M. J., & Calvert, P. P. (1975) *J. Cryst. Growth 30*, 343–351.
Phipps, L. W. (1964) *Trans. Faraday Soc. 60*, 1873–1883.
Rothblat, G. H., Rosen, J. M., Insull, W., Jr., Yau, A. O., & Small, D. M. (1977) *Exp. Mol. Pathol. 26*, 318–324.
Skoda, W., & Van den Tempel, M. (1963) *J. Colloid Sci. 18*, 568–584.
Small, D. M. (1986) *Handb. Lipid Res. 4*, 395–473.
Small, D. M., & Shipley, G. G. (1974) *Science (Washington, D.C.) 185*, 222–229.
Snow, J. W., McCloskey, H. M., Glick, J. M., Rothblat, G. H., & Phillips, M. C. (1988) *Biochemistry 27*, 3640–3646.
Turnbull, D. (1952) *J. Chem. Phys. 20*, 411–424.
Turnbull, D., & Fisher, J. C. (1949) *J. Chem. Phys. 17*, 71–73.
Volmer, M., & Weber, A. (1926) *Z. Phys. Chem. 119*, 277–301.
Wolfbauer, G. J. M., Minor, L. K., & Rothblat, G. H. (1986) *Proc. Natl. Acad. Acad. Sci. U.S.A. 83*, 7760–7764.

Localization of α1→3-Linked Mannoses in the N-Linked Oligosaccharides of *Saccharomyces cerevisiae mnn* Mutants†

Eugenio Alvarado, Lun Ballou, Luis M. Hernandez,‡ and Clinton E. Ballou*
Department of Biochemistry, University of California, Berkeley, California 94720
Received September 13, 1989; Revised Manuscript Received October 31, 1989

ABSTRACT: Neutral and phosphorylated N-linked oligosaccharides were isolated from *Saccharomyces cerevisiae mnn9* and *mnn9 gls1* mutant mannoproteins and separated into homologues that differed in the number of terminal α1→3-linked mannoses. In each type of oligosaccharide, the addition of such mannose was shown to occur in an ordered rather than a random fashion. The results confirm and extend an earlier report that dealt with the N-linked oligosaccharides from yeast invertase [Trimble, R. B., & Atkinson, P. H. (1986) *J. Biol. Chem. 261*, 9815–9824], and they suggest that the postulated processing pathway can be generalized to include phosphorylated and glucose-containing N-linked oligomannosides. We conclude that this processing pathway is identical for the analogous oligosaccharides from the *mnn9* and wild-type strains of *S. cerevisiae*. Analysis of the *mnn2 mnn10* mannoprotein revealed that a similar modification occurred at the branched terminus of the outer chain as well as in the core in this mutant.

The *mnn9*[1] mutant of *Saccharomyces cerevisiae* is a glycosylation-defective strain that makes mannoproteins that lack most of the outer chain portion of N-linked oligosaccharides (Ballou et al., 1980; Tsai et al., 1984a,b). A second glycosylation-defective mutant, called *mnn1*, lacks terminal α1→3-linked mannoses on both O- and N-linked oligosaccharides and on both the core and outer chain of the latter (Antalis et al., 1973; Raschke et al., 1973). The double mutant, *mnn1*

† This work was supported in part by National Science Foundation Grant PCM87-03141 and National Institutes of Health Grant AI-12522.
* To whom correspondence should be addressed.
‡ Visiting scholar from the Department of Microbiology, University of Extremadura, Badajoz, Spain.

[1] Abbreviations: M or Man, mannose; GlcNAc, *N*-acetylglucosamine; HOHAHA, homonuclear Hartmann–Hahn spectroscopy; ROESY, rotating-frame Overhauser enhancement spectroscopy; *mnn*, yeast mutant defective in protein glycosylation; H-1, H-2, and H-3, sugar ring protons, not to be confused with ^1H, ^2H, and ^3H; HPLC, high-performance liquid chromatography.

0006-2960/90/0429-2471$02.50/0